Available online at www.sciencedirect.com
ScienceDirect
Journal of Power Sources 163 (2007) 713–718
JOURNAL OF POWER SOURCES
www.elsevier.com/locate/jpowsour

Short communication

Electrochemical study of the formation of a solid electrolyte interface on graphite in a $LiBC_2O_4F_2$-based electrolyte

Sheng Shui Zhang *

U.S. Army Research Laboratory, AMSRD-ARL-SE-DC, Adelphi, MD 20783-1197, USA

Received 6 August 2006; received in revised form 14 September 2006; accepted 15 September 2006
Available online 7 November 2006

Abstract

The formation of a solid electrolyte interface (SEI) on the surface of graphite in a $LiBC_2O_4F_2$-based electrolyte was studied by galvanostatic cycling and electrochemical impedance spectroscopy (EIS). The results show that a short irreversible plateau at 1.5–1.7 V versus Li^+/Li was inevitably present in the first cycle of graphite, which is attributed to the reduction of $–OCOCOO^-$ pieces as a result of the chemical equilibrium of oxalatoborate ring-opening. This is the inherent property of $LiBC_2O_4F_2$ and it is independent of the type of electrode. EIS analyses suggest that the reduced products of $LiBC_2O_4F_2$ at 1.5–1.7 V participate into the formation of a preliminary SEI. Based on the distribution of the initial irreversible capacity and the correlation of the SEI resistance and graphite potential, it was concluded that the SEI formed at potentials below 0.25 V during which the lithiation takes place is most responsible for the long-term operation of the graphite electrode in Li-ion batteries. In addition, the results show that the charge-transfer resistance reflects well the kinetics of the electrode reactions, and that its value is in inverse proportion to the differential capacity of the electrode.
Published by Elsevier B.V.

Keywords: Lithium oxalyldifluoroborate; Lithium bis(oxalato)borate; Electrochemical impedance spectroscopy; Solid electrolyte interface; Graphite

1. Introduction

Lithium oxalyldifluoroborate (LiODFB, having a molecular formula of $LiBC_2O_4F_2$) was recently studied as an alternative salt to lithium bis(oxalato)borate (LiBOB) that has been known to strongly facilitate the formation of solid electrolyte interface (SEI) on the surface of carbonaceous anode materials [1–5]. Extensive spectroscopic analysis of the SEI formed with LiBOB electrolytes [4,5] has indicated that the enhanced stability is likely due to the participation of oxalatoborate molecular moieties in the SEI chemistry. Since LiODFB has the same oxalatoborate anhydride structure as LiBOB, most of the unique characteristics of LiBOB in Li-ion batteries have been found from LiODFB [1]. Beside this, LiODFB is superior to LiBOB in many other properties, for example, (1) it is more soluble in linear carbonate solvents that are essential to lower viscosity and increase wettability of the Li-ion electrolytes, (2) it results in a less irreversible capacity at about 2 V in the first cycle of Li-ion cell due to the lower concentration of the oxalate group in its molecule, and (3) the Li-ion cell using it has a better power capability and low temperature cyclic performance. On the other hand, it was found that $LiBF_4$-based electrolytes are able to provide Li-ion batteries with better low temperature performance than the $LiPF_6$ counterparts in spite of the known low ionic conductivity of the $LiBF_4$-based electrolytes [6,7]. These merits are attributed to the reduced charge-transfer resistance of $LiBF_4$ cells. Ascribed to the unique chemical structure of LiODFB, the combined advantages of LiBOB and $LiBF_4$ electrolytes have been obtained from the LiODFB-based electrolyte [1], which include: (1) the optimized ionic conductivity over a wide temperature range, (2) the ability to provide a high cycling efficiency for metallic lithium plating and stripping on the surface of Cu, a current collector material of the graphite anode, (3) excellent ability to passivate Al at high potentials, (4) the ability to support graphite cycling in high PC-containing solutions, (5) the ability to support Li-ion cell operating at high temperatures, (6) the ability to support Li-ion cell delivering high capacity at low temperatures and high current rates, and (7) the possibility to provide safety protection against abuse operations.

* Tel.: +1 301 394 0981; fax: +1 301 394 0273.
E-mail address: szhang@arl.army.mil.

0378-7753/$ – see front matter. Published by Elsevier B.V.
doi:10.1016/j.jpowsour.2006.09.040

As a continuous effort, in this work the SEI formation of graphite anode in a LiODFB electrolyte will be studied by galvanostatic cycling and electrochemical impedance spectroscopy (EIS). The SEI formation will be discussed in terms of the irreversible capacity and cell impedance with respect to the potential of graphite in the first cycle.

2. Experimental

LiODFB was synthesized by the reaction of BF_3 etherate and $Li_2C_2O_4$ in a 1:1 molar ratio and purified through extraction and recrystallization using dimethyl carbonate as the solvent. The detailed procedure and characterization of LiODFB were described previously [1]. Solvents of propylene carbonate (PC, Grant Chemical), ethylene carbonate (EC, Grant Chemical), and ethylmethyl carbonate (EMC, EM Industries) were dried over 4 Å molecular sieves until the water content was lower than 20 ppm, as determined by Karl-Fisher titration. The standard Gen. 3 electrodes of the DOE ATD program, provided by Argonne National Laboratory, were used. The graphite anode was composed of 90% MCMB 10–28, 2% VGCF (a conductive carbon fiber), and 8% PVDF binder, and the cathode of 84% $LiNi_{1/3}Mn_{1/3}Co_{1/3}O_2$ (hereafter abbreviated as NMC), 8% carbon black, and 8% PVDF binder (all were weight percentage). The electrodes were punched into small discs with an area of 1.27 cm^2 and dried at 110 °C under vacuum for 16 h prior to use. Using the salt and solvents above, a 1.0 m (molality, mole salt per kilogram solvent) LiODFB 1:1:3 (wt.) PC/EC/EMC electrolyte was prepared in an argon-filled glove-box. A 3-electrode button cell with metallic Li foil as the reference electrode was assembled and filled with 80 μl of liquid electrolyte in the same glove-box. A schematic diagram of the 3-electrode button cell is shown in Fig. 1. To build the reference electrode, a small piece of thin Li foil was pressed onto one end of a strip of 0.125 mm thick Ni foil (Aldrich) and wrapped with Celgard® separator. The reference electrode was placed between two separators that isolated the electrodes, and the cell was hermetically crimped using a Rayovac Miltipress in a dry-room with dew point of about −90 °C. In addition, an electrolyte-flooded cell with Cu wire as the working electrode and Li foil as the counter and reference electrode, respectively, was assembled for cyclic voltammery. The working electrode was made by wrapping a freshly polished Cu wire (1.2 mm in diameter) with a thermal shrinkable Teflon® tube and leaving a 1.0 cm length of Cu wire exposed to the liquid electrolyte.

Galvanostatic cycling experiments were conducted on a Maccor Series 4000 tester. In addition to cycling the cell, the other two channels were used to record the potentials of the cathode and anode, separately. A detailed description and connection circuitry were described elsewhere [8]. A Solartron SI 1287 Electrochemical Interface and a SI 1260 Impedance/Gain-Phase Analyzer, controlled by CorrWare and Zplot Softwares, were used for the measurements of cyclic voltammery and electrochemical impedance spectroscopy. The EIS was potentiostatically measured at a specific voltage with an ac oscillation of 10 mV amplitude over the frequencies from100 kHz to 0.01 Hz. The voltage at which the EIS was measured was achieved by cycling the cell at a constant current density of 0.15 mA cm^{-2}. The collected EIS data was fitted using ZView software. All tests were carried out at room temperature (∼23 °C).

3. Results and discussion

3.1. Electrochemical characteristic of the first cycle

Fig. 2 exhibits the responses of cell voltage and electrode potentials to the cycling time, which were recorded from the first cycle of a graphite/LiODFB electrolyte/NMC Li-ion cell at a current rate of 0.1C (0.15 mA cm^{-2}). Without exception, a short plateau of about 20 min near 2 V was inevitably present in the LiODFB Li-ion cell. As indicated in the inset of Fig. 2, this short plateau is entirely related to the graphite anode, instead of the cathode. In addition, the potential of the graphite anode at the end of charging was 0.056 V versus Li^+/Li, which means that the graphite anode could not been fully lithiated in the present Li-ion cell. As a result, the coulombic efficiency of the first cycle was only 76%, being somewhat low as compared with those of the normal Li-ion cells. This phenomenon is attributed to the

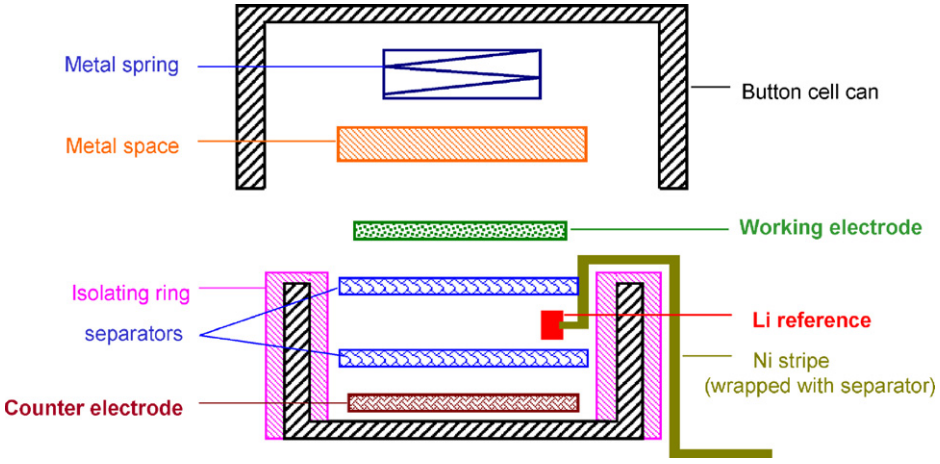

Fig. 1. A schematic view of the 3-electrode button cell.

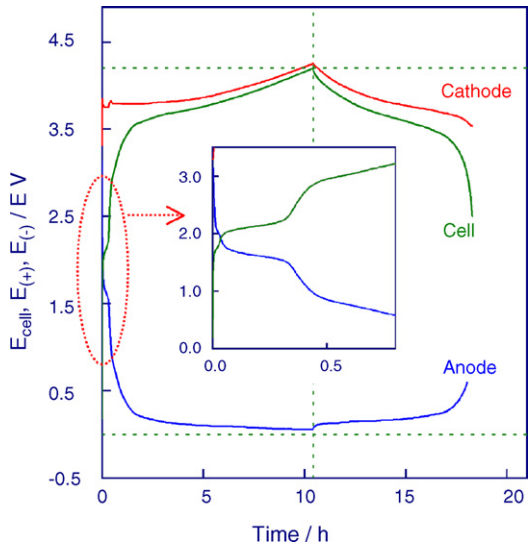

Fig. 2. Cell voltage and electrode potentials of the first cycle of a graphite/LiODFB electrolyte/NMC Li-ion cell as a function of cycling time, which were recorded at 0.15 mA cm^{-2} by using three independent channels. Inset is an enlargement of the initial period.

unbalanced capacity ratio (C/A ratio) of the cathode to the anode. Based on the reversible capacities of Li/graphite and Li/NMC half-cells, the C/A ratio in the presenct case was estimated to be 0.762, which is a little lower than the normal value [8]. In this work, therefore, a Li/graphite half-cell was selected for the further evaluation so that the SEI formation of graphite in whole the lithiation potentials can be recorded.

Fig. 3 shows potential–capacity and differential capacity–potential correlations of the graphite electrode, which were plotted based on the data of the first cycle of a Li/graphite half-cell. The initial coulombic efficiency of graphite was evaluated from Fig. 3 to be 85.6% (i.e., 14.4% irreversible loss), being about 10% higher than that obtained from Li-ion cell as described above. According to the differential capacity-potential correlation in Fig. 3, the initial irreversible loss may be divided into two potential stages: the first stage was generated in the potential region of above 0.3 V, in which lithiation did not take place, and the second stage was produced in the potential region of below 0.3 V, in which lithiation occured. Based on this criterion, the irreversible capacity in the first stage was 5.3% and

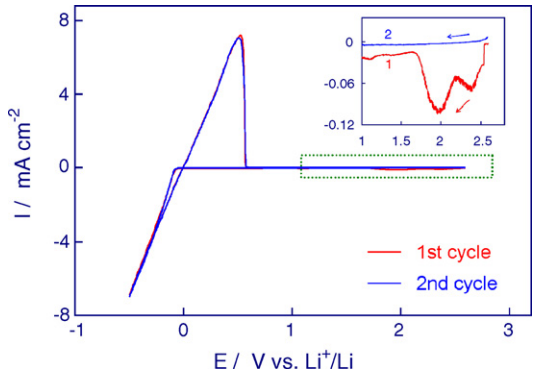

Fig. 4. Cyclic voltammograms of the first two cycles of a Cu electrode flooded in a LiODFB electrolyte, which were recorded at a potential scanning rate of 5 mV s^{-1}. Note that the cyclic voltammograms of two cycles are so close that they are overlapped with each other, and that the inset is an enlargement of the selected part, as marked in figure.

that in the second stage was 9.1%. Generally, the first stage was related to the irreversible reduction of electrolyte components such as solvents and salt, which resulted in the formation of a preliminary SEI and the resulting SEI was highly porous and instable. The second stage was associated with the irreversible reduction of both electrolyte components and surface chemical groups of graphite, and the resulting SEI was structurally compact and stable [9–11].

It is also shown in Fig. 3 that the short potential plateau, which corresponds to the one near 2 V in Li-ion cell, was present at 1.5–1.7 V versus Li$^+$/Li in Li/graphite half-cell, and that this plateau disappears in the second cycle and later (not shown in figure). To clarify the mechanism resulting in this irreversible plateau (reduction), a Cu electrode was used as an alternative electrode to examine the electrolyte. The resulting cyclic voltammograms of the first two cycles are plotted in Fig. 4. Since the reversibility of plating and stripping of metallic Li in LiODFB electrolyte was so high, the two cyclic voltammograms overlapped each other. However, the initial irreversible reduction also was observable in the enlarged part of the cyclic voltammograms, as shown in the inset of Fig. 4. This fact verifies that the short 2 V-plateau observed in the first cycle of Li-ion cell is directly linked to the inherent properties of LiODFB, regardless of the type of electrodes. In solution, LiODFB simultaneously undergoes two chemical equilibriums (1) and (2), as

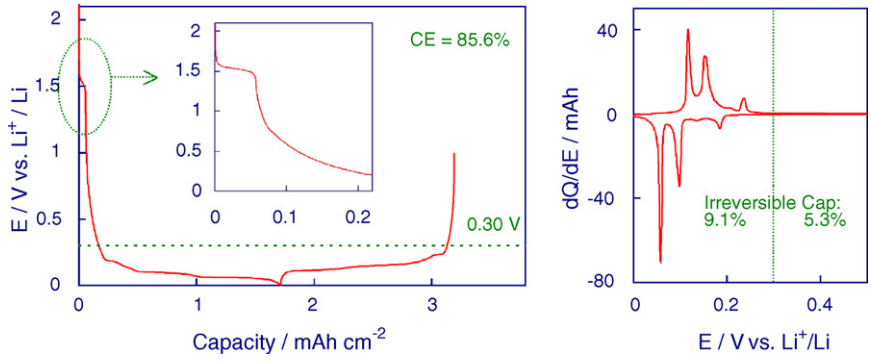

Fig. 3. Potential–capacity and differential capacity–potential plots of the first cycle of a 3-electrode Li/LiODFB electrolyte/graphite button cell, which were drawn from the data recorded at 0.15 mAh cm^{-2}.

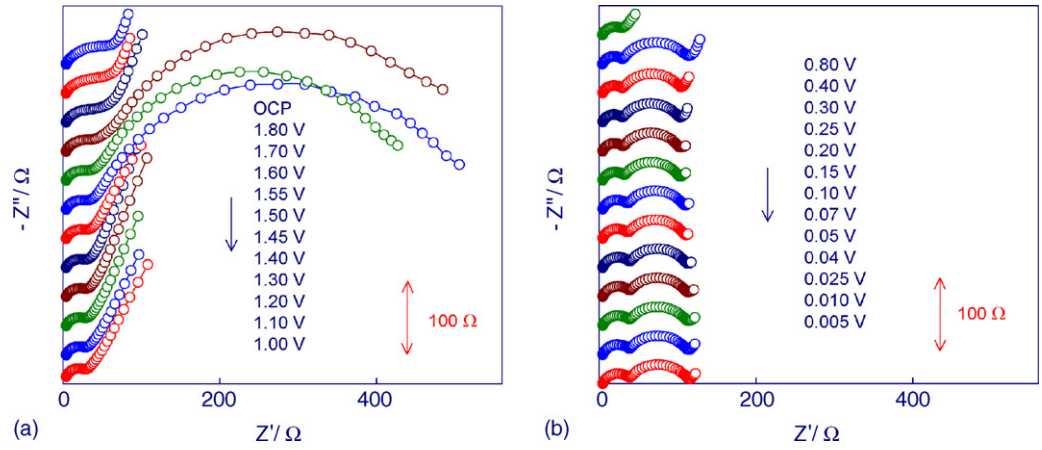

Fig. 5. EIS of graphite electrode in a LiODFB electrolyte at various potentials, which were recorded during the first lithiation process: (a) from OCP (i.e., freshly assembled cell at open circuit potential) to 1.0 V and (b) from 0.8 to 0.005 V.

shown below:

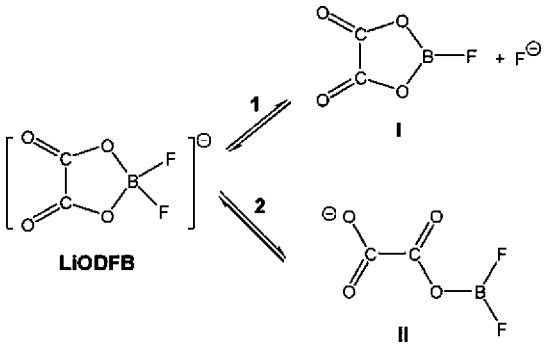

where the –OCOCOO$^-$ piece in anion (II) as a result of oxalatoborate ring-opening is responsible for the 2 V-plateau in Li-ion cell. A similar phenomena with the same reason also has been observed in the case of LiBOB-based electrolytes [3,4,12]. It should be mentioned that, in addition to the inherent properties of LiODFB, the presence of moisture and oxalate-related impurities would remarkably increase the length of the irreversible 2 V-plateau in the first cycle. Therefore, both the moisture and oxalate-related impurities should be strictly controlled in the salt synthesis and electrolyte preparation so that good performance of LiODFB-based Li-ion batteries can be achieved.

3.2. EIS model of the graphite electrode

The EIS of a Li/LiODFB electrolyte/graphite half-cell at various potentials are plotted in Fig. 5a and b. In all cases, the EIS show either one semicircle or two partially overlapped semicircles, followed by a straight sloping line at the low frequency end. Such patterns of EIS can be fitted using an equivalent circuit shown in Fig. 6 [13–16]. R_b is bulk resistance of the cell, which reflects a combined resistance of the electrolyte, separator, and graphite electrode. R_{sei} and C_{sei} are resistance and capacitance of the SEI on the surfaces of graphite, which correspond to the semicircle at high frequencies. R_{ct} and C_{dl} are the charge-transfer resistance and its relative double-layer capacitance, which correspond to the semicircle at medium frequencies. W is the Warburg impedance related to a combined effect of the diffusion of lithium ions on the electrode–electrolyte interface, which corresponds to the straight sloping line at low frequency end. Since the R_b and R_{sei} are of ohmic characteristic, their combination is called an ohmic impedance. Whereas the charge-transfer impedance and Warburg impedance reflect electrochemical processes occurring on the electrode–electrolyte interface, and their combination is called as Faradaic impedance. Especially, the R_{ct} is more related to the kinetics of electrochemical reactions on the electrode. In the potential regions where no electrode reactions take place, the R_{ct} is so high that its related semicircle disappears, and in this case the EIS shows only one semicircle followed by a straight sloping line, as shown by most of EIS in Fig. 5a. Based on the fact that the R_{sei} is changed with the formation and growth of the SEI, the SEI formation of graphite can be studied in situ by using EIS technique.

3.3. Understanding of the SEI formation

The potential dependences of the differential capacity, R_b, R_{sei}, amd R_{ct} in the first cycle of a Li/graphite half-cell are plotted in Fig. 7, in which the R_b, R_{sei}, and R_{ct} in the tenth cycle are

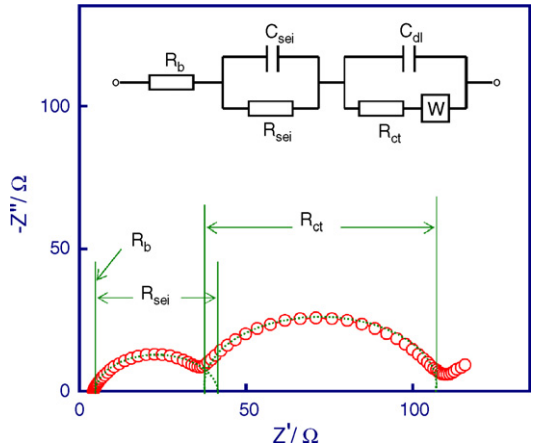

Fig. 6. An equivalent circuit used for the analyses of EIS. The shown EIS was recorded at 0.10 V.

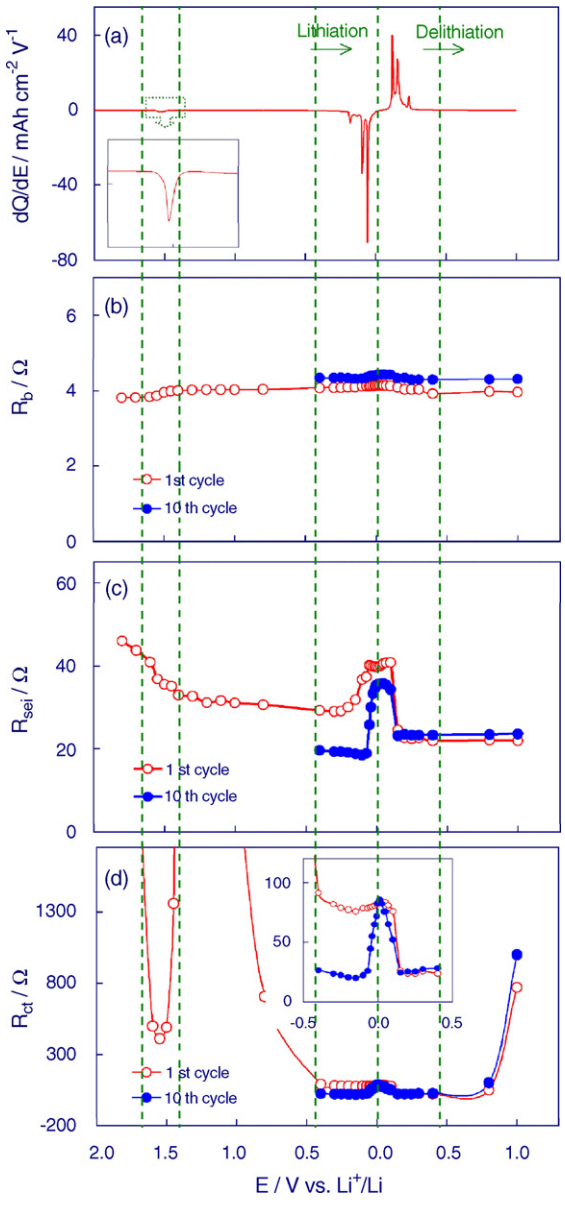

Fig. 7. Potential dependences of (a) differential capacity, (b) R_b, (c) R_{sei}, and (d) R_{ct} of the graphite electrode in a LiODFB electrolyte, which were plotted from the data of the first and tenth cycles at a current density of 0.15 mA cm^{-2}.

also plotted for the purpose of comparison. In general, the R_b was reversibly changed in a very small range with the lithiation and delithiation of graphite. This is ascribed to the reversible expansion and extraction of graphite electrode, which corresponded to the intercalation and deintercalation of Li^+ ions with graphite. The potential dependence of the R_{sei} was a much more complicated manner, which was affected not only by the SEI formation but also by the cycling process. To understand the R_{sei}–E correlation, the R_{sei} in the tenth cycle (Fig. 7c) in which the SEI formation has been complete is compared with the differential capacity (Fig. 7a). It is shown that the R_{sei} was increased considerably at ~0.07 V versus Li^+/Li in the lithiation process and decreased back to the original level at ~0.15 V versus Li^+/Li in the following delithiation process. Such changes are ascribed to the reversible expansion and extraction of the graphite electrode, as indicated by the excellent corresponding correlation between the differential capacity and R_{sei} in Fig. 7a and c, respectively.

The R_{sei}–E correlation in the first cycle consists of three potential regions. The first potential region was around 1.5 V and higher, which corresponds to the short 1.5–1.7 V-plateau in Fig. 3. Due to the reduction of the –OCOCOO$^-$ pieces originating from the chemical equilibrium of LiODFB (as shown in the inset of Fig. 7a), the R_{sei} was remarkably decreased and the reduced R_{sei} was remained in lower potentials (Fig. 7c). This observation suggests that the reduced products of LiODFB must be retained as a component of the preliminary SEI on the graphite surface. The second potential region was between 1.5 and 0.25 V, during which the reduction of electrolyte solvents underwent but the lithiation did not take place. In the second potential region, the R_{sei} was decreased gradually with the decrease of potential, which reflected the growth of the preliminary SEI being highly porous, less conductive, and probably unstable [9,11]. The third potential region was below 0.25 V, during which the lithiation process took place, as indicated by three peaks of the differential capacities in Fig. 7a. The R_{sei}–E correlation in the third potential region is affected by two opposite effects [11]: (1) the formation of the highly conductive SEI, which results in a decrease of the R_{sei}, and (2) the expansion of graphite electrode, which leads to an increase of the R_{sei}. Depending on the interaction of these two opposite effects, the R_{sei} may decrease, increase, or remain unchanging with the decrease of graphite potential [11]. In the present case, the second factor was more significant than the first one. Therefore, the R_{sei} showed a little smaller increase with the decrease of the graphite potential, as compared with that observed in the tenth cycle (Fig. 7c). Considering the distribution of the initial irreversible capacity as discussed in Section 3.1, one finds that the first and second potential regions produced a total 5.3% of irreversible capacity, while the third region up to 9.1%. This fact suggests that the third potential region play an important role in the SEI formation, and that the SEI formed in the third potential region is most responsible for the long-term operation of graphite anode in the Li-ion batteries.

Like other cases observed from Li/graphite cells [9,12], Li/cathode cells [17,18], and Li-ion full cell [19], the R_{ct} reflects the kinetics of the electrochemical reactions on the graphite electrode. A general rule is that the R_{ct} is in inverse proportion to the differential capacity or the current in a cyclic voltammogram [12,19]. It can be seen from Fig. 7d and its inset that the R_{ct} in the first lithiation process appeared two minima at ~1.5 and ~0.1 V, respectively, and that the second one reversibly showed up at ~0.15 V in the following delithiation process. Comparing Fig. 7a and d, one finds that the changes of the R_{ct} and differential capacity with the potential are consistent with each other.

4. Conclusions

Based on the results of this work, it may be concluded that (1) the short irreversible plateau at 1.5–1.7 V versus Li^+/Li in the first cycle of graphite is due to the inherent properties of LiODFB, regardless of the type of the electrodes, (2) the reduction of LiODFB at 1.5–1.7 V participates into the formation of a preliminary SEI, which is accompanied by a remarkable

decrease of the R_{sei}, (3) According to the R_{sei}–E correlation, the SEI formation can be divided into three potential regions: (a) above 1.5 V, (b) 1.5–0.25 V, and (c) below 0.25 V, (4) the SEI formed in the potentials of below 0.25 V is most responsible for the long-term operation of the graphite anode, (5) the R_{sei}–E correlation in the potentials of below 0.25 V is affected by two opposite effects: (a) the formation of the highly conductive SEI, which results in R_{sei} decreasing, and (b) the expansion of the graphite electrode, which leads to the R_{sei} increasing, and (6) the R_{ct} reflects the kinetics of electrode reactions, and its value is in reverse proportion to the differential capacity of the electrode.

Acknowledgment

Receipt of the electrodes from Argonne National Laboratory is gratefully acknowledged.

References

[1] S.S. Zhang, Electrochem. Commun. 8 (2006) 1423.
[2] K. Xu, S.S. Zhang, B.A. Poese, T.R. Jow, Electrochem. Solid-State Lett. 5 (2002) A259.
[3] K. Xu, S.S. Zhang, T.R. Jow, Electrochem. Solid-State Lett. 6 (2003) A117.
[4] K. Xu, U. Lee, S.S. Zhang, M. Wood, T.R. Jow, Electrochem. Solid-State Lett. 6 (2003) A144.
[5] G.V. Zhuang, K. Xu, T.R. Jow, P.N.J. Ross, Electrochem. Solid-State Lett. 7 (2004) A224.
[6] S.S. Zhang, K. Xu, T.R. Jow, Electrochem. Commun. 4 (2002) 928.
[7] S.S. Zhang, K. Xu, T.R. Jow, J. Solid State Electrochem. 7 (2003) 147.
[8] S.S. Zhang, K. Xu, T.R. Jow, J. Power Sources 160 (2006) 1349.
[9] S.S. Zhang, M.S. Ding, K. Xu, J. Allen, T.R. Jow, Electrochem. Solid-State Lett. 4 (2001) A206.
[10] E. Peled, C. Menachem, D. Bar-Tow, A. Melman, J. Electrochem. Soc. 143 (1996) L4.
[11] S.S. Zhang, K. Xu, T.R. Jow, Electrochim. Acta 51 (2006) 1636.
[12] K. Xu, S.S. Zhang, T.R. Jow, J. Power Sources 143 (2005) 197.
[13] N. Takami, A. Satoh, M. Hara, T. Ohsaki, J. Electrochem. Soc. 142 (1995) 371.
[14] T. Piao, S.M. Park, C.H. Doh, S.I. Moon, J. Electrochem. Soc. 146 (1999) 2794.
[15] Y.C. Chang, J.H. Jong, G.T. Fey, J. Electrochem. Soc. 147 (2000) 2033.
[16] T.S. Ong, H. Yang, Electrochem. Solid-State Lett. 4 (2001) A89.
[17] S.S. Zhang, K. Xu, T.R. Jow, Electrochem. Solid-State Lett. 5 (2002) A92.
[18] S.S. Zhang, K. Xu, T.R. Jow, J. Electrochem. Soc. 149 (2002) A1521.
[19] S.S. Zhang, K. Xu, T.R. Jow, Electrochim. Acta 49 (2004) 1057.